Theor Chem Acc (2003) 109:160–168
DOI 10.1007/s00214-002-0424-0

Theoretical
Chemistry Accounts

Regular article

Quantum mechanics and mixed quantum mechanics/molecular mechanics simulations of model nerve agents with acetylcholinesterase

M.M. Hurley[1], J.B. Wright[2], G.H. Lushington[3], W.E. White[4]

[1] US Army Research Laboratory, AMSRL-CI-HC, Aberdeen Proving Ground, MD 21005, USA
[2] US Army Natick Soldier Center, AMSSB-RSS-M, Kansas St., Natick, MA 01760, USA
[3] University of Kansas, 1251 Wescoe Hall Rd., c/o Dept. of Medicinal Chemistry, Lawrence, KS 66045, USA
[4] Edgewood Chemical Biological Center, 5183 Blackhawk Road, Aberdeen Proving Ground, MD 21010, USA

Received: 10 October 2001 / Accepted: 13 November 2002 / Published online: 1 April 2003

Abstract. The accurate modeling of biological processes presents major computational difficulties owing to the inherent complexity of the macromolecular systems of interest. Simulations of biochemical reactivity tend to require highly computationally intensive quantum mechanical methods, but localized chemical effects tend to depend significantly on properties of the extended biological environment – a regime far more readily examined with lower-level classical empirical models. Mixed quantum/classical techniques are gaining in popularity as a means of bridging these competing requirements. Here we present results comparing two quantum mechanics/molecular mechanics implementations (the SIMOMM technique of Gordon et al. as implemented in GAMESS, and the ONIOM technique of Morokuma et al. found in Gaussian 98) as performed on the enzyme acetylcholinesterase and model nerve agents. This work represents part of the initial phase of a DoD HPCMP Challenge project in which we are attempting to reliably characterize the biochemical processes responsible for nerve agent activity and inhibition, thereby allowing predictions on compounds unrelated to those already studied.

Keywords: Acetylcholinesterase – IMOMM – Nerve agent – Simulation

Contribution to the Proceedings of the Symposium on Combined QM/MM Methods at the 222nd National Meeting of the American Chemical Society, 2001

Correspondence to: M. M. Hurley
e-mail: hurley@arl.army.mil

Introduction

The enzyme acetylcholinesterase (AChE) has been a topic of interest to theoreticians and experimentalists alike for a number of years. A large amount of this effort in the medical and academic communities has been in the course of investigating diseases such as Alzheimer's and myasthenia gravis. However, the enzyme has remained of key interest for military and civilian security personnel for the role it plays in nerve agent activity and inhibition. AChE and the related enzyme butyrylcholinesterase each catalyze the hydrolysis of the neurotransmitter acetylcholine in a two-step sequence. In the transesterification reaction, the acetate moiety is transferred from the choline to a serine residue on the active site of the enzyme. Water then hydrolyzes the acetylated serine to form acetic acid and regenerates the enzyme for subsequent catalysis (Fig. 1) [1]. Both nerve agents and organophosphorus pesticides function by inhibiting the enzyme [2], leading to the uncontrolled accumulation of acetylcholine at the neuro–neuro and neuro–muscular junctions, causing a wide variety of life-threatening symptoms [3, 4].

A key feature of the enzyme active center is the catalytic triad, which consists of serine-200, histidine-440, and glutamate-327 (residue numbering according to *Torpedo Californica* AChE structure [5]). An important aspect of the catalysis is the facile formation of the nucleophilic serine anion. To form this anion, a proton is transferred from the hydroxyl group on Ser200 to a nitrogen atom in the imidazole ring of His440. Simultaneously, a proton is transferred from the other nitrogen in the ring to the carboxyl group on Glu327. This proton transfer is expected to proceed concurrently with the nucleophilic attack on the carbonyl group of acetylcho-

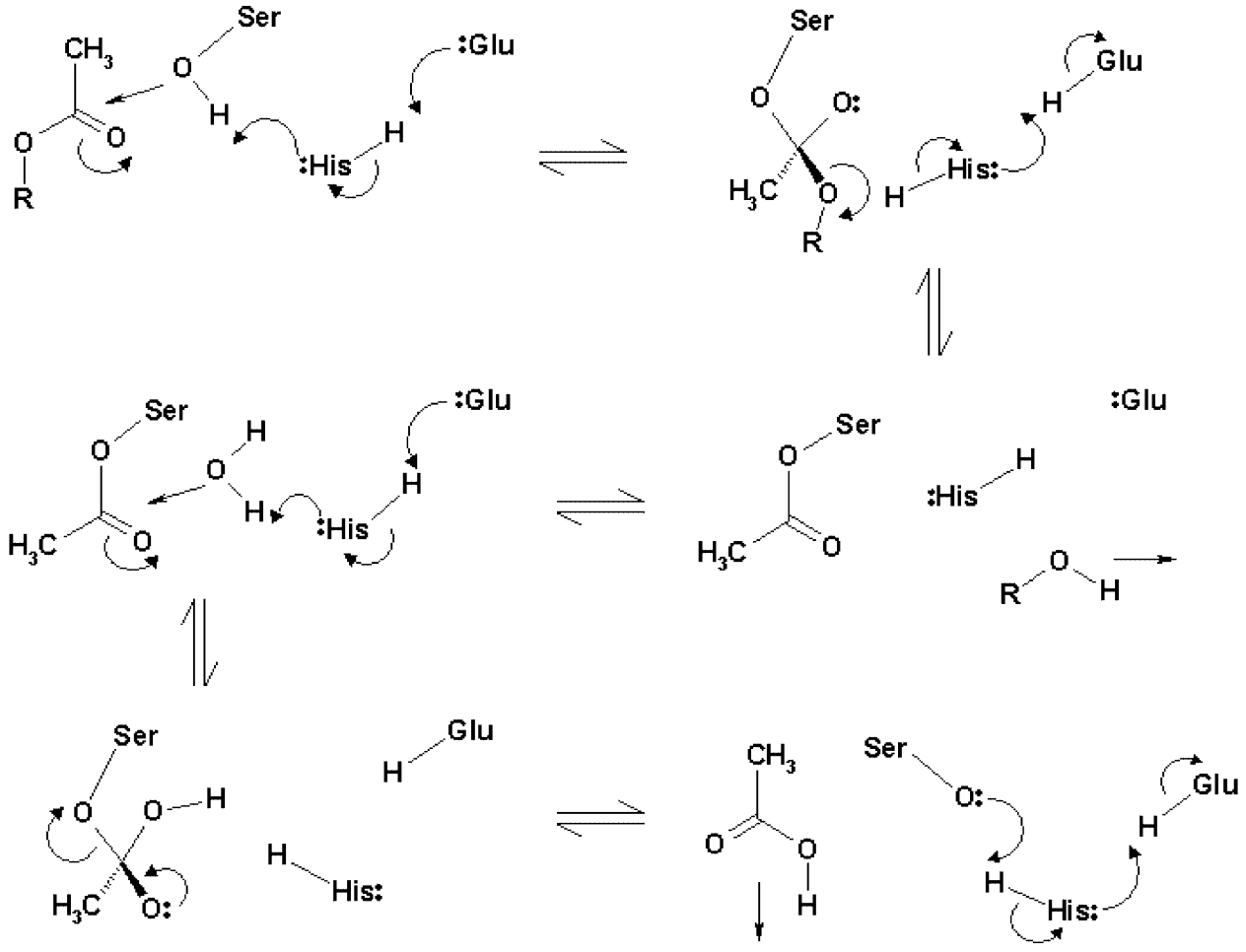

Fig. 1. Schematic of acetylcholinesterase (*AChE*)-catalyzed hydrolysis of acetylcholine

line (or the phosphinyl group on dimethylphosphinic fluoride as depicted in Fig. 2). An important additional structural feature is the nearby oxyanion hole (Gly118, Gly119, and Ala201 in the *Torpedo* numbering), which performs the function of stabilizing the negative charge developing on the anionic moiety of the ligand.

As is the case for carbonyl esters, the serine anion is capable of attacking phosphorus esters and carbamates. Unfortunately, water does not have sufficient nucleophilic strength to hydrolyze the phosphylated or carbamalated serine. Thus, with these substrates, the enzyme active site becomes blocked and is unable to catalyze further hydrolysis of acetylcholine.

During the last half century, considerable empirical data has emerged regarding the substrate/activity relationships of AChE, rates of inhibition, and nucleophiles for removing the adducts, and a considerable body of literature pertaining to agent toxicity and prophylaxis has evolved [6, 7, 8, 9]. However, a detailed understanding of the mechanistic underpinnings and systematic anatomization of AChE inhibition, regeneration, and aging has remained elusive, in part owing to the system size and complexity. Many early approaches entailed semiempirical calculations on a truncated trypsin enzyme containing the active center and a few additional amino acids [10]. The main alternatives to semiempirical methods have been the fully empirical techniques such as classical molecular dynamics (MD) and molecular mechanics (MM) wherein the entire protein may be studied, but at the expense of omitting explicit electronic structural effects that are fundamental to reliable prediction of chemical reactivity [11, 12].

Among the most important prior efforts in AChE activity modeling is that of Bencsura et al. [13], who employed a variety of techniques (including MM, MD and ab initio quantum chemical formalisms) to study AChE substrate binding and transition-state (TS) structure. Via quantum chemical means, it was possible to determine a candidate structure for a prospective pentavalent TS and to develop a classical force field from those calculations. The pentavalent phosphonate was then placed inside the enzyme active site, and binding to the neighboring amino acid residues was studied. These latter studies were fundamentally limited, however, in that the absence of explicit electronic structural information in the classical model precluded a reliable simulation of bond breakage and activation energy prediction for the reaction.

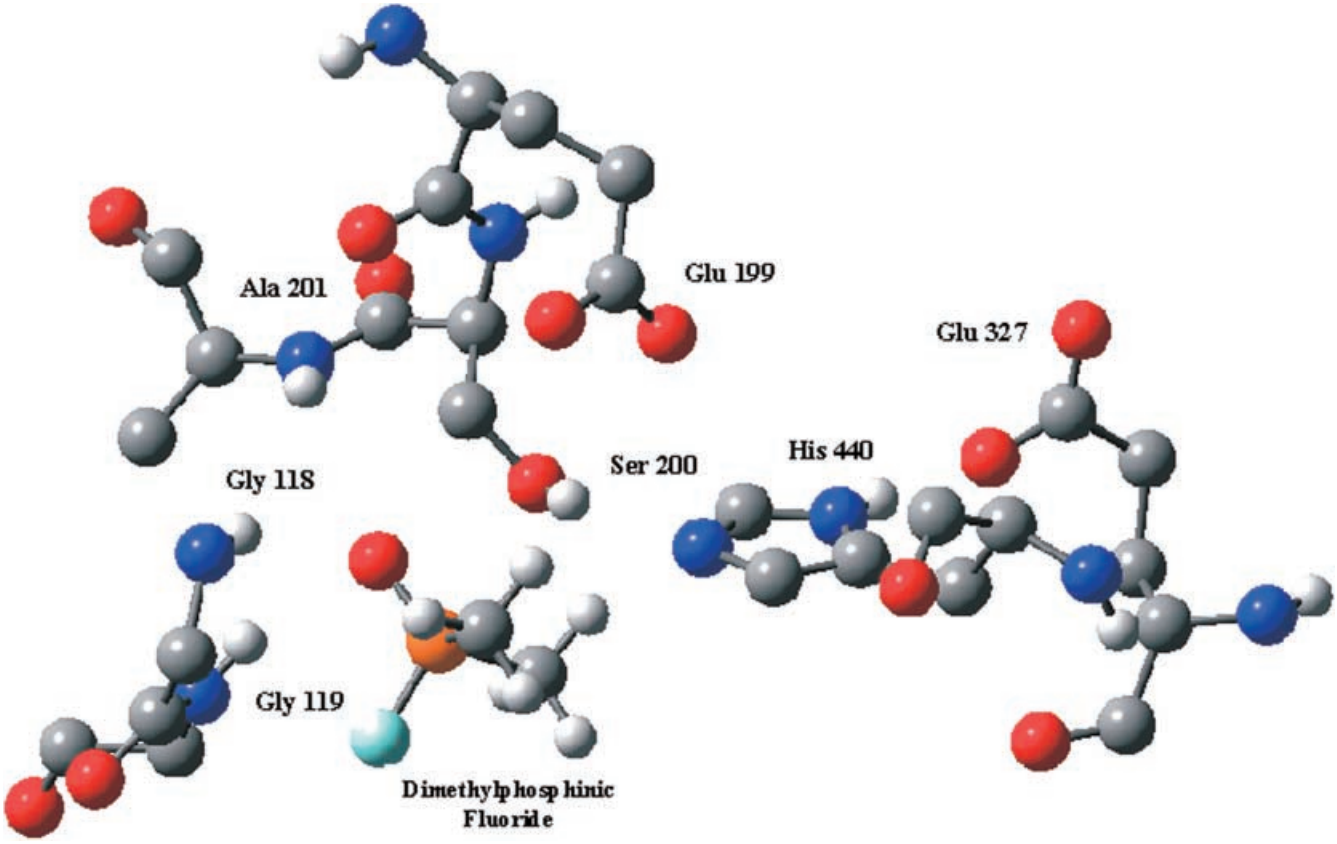

Fig. 2. Significant residues of the active site of AchE and dimethylphosphinic fluoride. For simplicity, only the significant protons are depicted. The catalytic triad consists of Ser200, His440, and Glu327. The oxyanion hole consists of Gly118, Gly119, and Ala201. The Ser200 hydroxyl group is lined up opposite to the phosphinate fluoride. The phosphinyl group is coordinated in the oxyanion hole

Additional formidable MD work on AChE has been performed by Tai and coworkers [14, 15] to address complex structural issues involving solvation, the hypothetical "back door" to the active site, and gating of the gorge.

While classical MD work and truncated quantum mechanics (QM) models of AChE have been the rule, a notable exception is the QM/MM work of Vasilyev [16], who used a combination of PM3 and the OPLS force-field to study protonation within the catalytic triad, as well as inhibition by a simple organophosphate $P(F)(O)(NH_2)(CH_3)$. It is important to note that in this model only the catalytic triad sidechains and the substrate were studied at the quantum level, and the surrounding enzyme environment was held fixed.

Similar enzyme processes have been the focus of theoretical studies performed with a variety of clever techniques to obviate the problems associated with inadequate computer power. Of particular interest is a recent QM/MM study of the catalytic mechanism for citrate synthase [17], which is relevant to the current effort as it involves the transfer of a methyl proton on acetyl CoA to asparate-375 and the possible protonation of the carbonyl oxygen by histidine-274. Also extremely relevant are the QM/MM studies of Topf et al. [18] on the deacylation step of the serine protease elastase.

This paper represents initial results in an attempt to use QM/MM methodologies to provide accurate and reliable characterization of nerve agent activity and inhibition of the AChE active site. Two methodologies, the ONIOM method of Dapprich et al. [19] and the related SIMOMM method of Shoemaker et al. [20], are used to study both bare AChE and a series of systems involving model nerve agent ligands. The roles of model size, forcefield, and methodology are examined, as well as the chemical structure of the catalytic triad (including the existence of the short, strong hydrogen bond or SSHB), which are a vital aspect of the efficacy of the enzyme. QM and QM/MM layer calculations are also performed on smaller models involving model nerve agents and the active site area residues to investigate energetics, TS formation, and the role of the oxyanion hole.

Methods

The IMOMM (and related) methodology of Maseras and Morokuma [21] was one of the early QM/MM implementations available to the nonspecialist user. A number of academic and commercial codes still rely on permutations of this algorithm. ONIOM calculations in this work have been performed using the Gaussian codes [22]. This work has been performed on several size models of the AChE active site, both with and without a model nerve agent. In addition, these results have been augmented by calculations performed using

the IMOMM-based SIMOMM method of Shoemaker et al. as implemented in the GAMESS-US code [23]. This implementation uses the Tinker package of Pappu et al. [24] for the MM component. One of the major conceptual differences between ONIOM and SIMOMM lies in the treatment of atoms in the MM region that are directly bound to the QM region (which will be referred to here as "boundary atoms"), and in the treatment of the atoms (typically hydrogens) added to the QM region to terminate dangling bonds. Boundary atoms in ONIOM represent a specific subset of the bulk region and are fixed during the optimization. In the SIMOMM method, boundary atoms are treated no differently than the rest of the MM region and are allowed to optimize in response to the MM gradient. Similarly, termination atoms in the QM region are fixed in the ONIOM method, yet optimized in SIMOMM in response to the QM gradient. It is the contention of the SIMOMM developers that this improves the calculation by removing user-defined constraints. Additional trivial differences arise in terms of available forcefields, etc. A preliminary comparison of the two methods will be given.

A number of reliable experimentally derived crystal structures for various forms of AChE are available. Crystal structures for both *T. Californica* and *Mus Musculus* obtained from the RCSB databank have been used to obtain starting structures. Several different size models have been used, ranging from a small model (containing only the active site residues plus model agent), to an intermediate model (containing the active site residues plus the oxyanion hole residues plus the model agent), to two larger models (composed of all residues which at least partially reside within a 7 or 10 Å radius of the active-site histidine, augmented with further residues to preserve natural ribbon contiguity). Methyl groups were added to terminal residue backbone nitrogens to truncate the chain. The Rasmol software was used to carve the model residues from the PDB file, and hydrogens were added to the structures using the protonate facility of AMBER. For the small and intermediate models, constraints were placed on terminal carbon atoms for each chain to keep the model intact. No optimization constraints were used on the 7 and 10 Å models. No explicit waters have been included in the model at this point. Concurrent work is underway to study the energetics of model agent hydrolysis in water, as well as model agent–enzyme interactions including explicit waters, which will be reported elsewhere.

Results and discussion

Bare enzyme

NMR studies of the AChE active-site structure suggest strong coupling between residues of the serine/histidine/glutamate catalytic triad in the form of strong hydrogen-bonding interactions. This hydrogen-bonded coupling is believed to be an essential factor in the proton-transfer processes that enhance the catalytic nucleophilicity of such enzymes [25]. Specifically, the serine hydroxyl hydrogen is believed to experience a strong electrostatic attraction by a nitrogen on the nearby histidine ring. This interaction is stabilized by a short strong hydrogen bond (SSHB) (alternatively known as a low-barrier hydrogen bond) between a nitrogenic proton on the histidine ring and the neighboring unprotonated glutamic acid residue, an arrangement for which proton NMR studies have predicted an O_{Glu}–N_{His} SSHB distance of around 2.64 ± 0.04 Å [25].

Calculations performed on the 10-Å model [SIMOMM; restricted Hartree–Fock, RHF, 6-31G(d) basis; AMBER forcefield] display the expected sensitivity of the catalytic triad structure to protonation state. Results with the His-N_δ protonated agree well with the experimentally resolved crystal structure (*M. Musculus* AChE 1MAA [26]) and display proper alignment of the triad. The structure with His-N_ϵ (and not His-N_δ) differs dramatically from both, however, in that the stabilizing influence of the hydrogen bond from the His-N_δ to the neighboring Glu327 has been removed, producing unphysical results. While we have carried out some mapping of structural fluctuations due to the protonation state in the course of benchmarking the models, the remainder of the work discussed here will be confined to the biologically relevant initial structure with His-N_δ protonated and Glu327 unprotonated.

In addition, the structure of the catalytic triad displays sensitivity to forcefield choice and model size. Major differences in results are seen in Fig. 3, in which the triad structure from an ONIOM 7-Å calculation is compared with SIMOMM 7 and 10-Å calculations [all done at the HF level using a 6-31G(d) basis set], where the SIMOMM runs were performed using the AMBER forcefield and the ONIOM results are obtained with the universal forcefield (UFF). The two protons relevant to the hydrogen-bonded coupling within the triad are depicted explicitly in the graphic, indicating that the

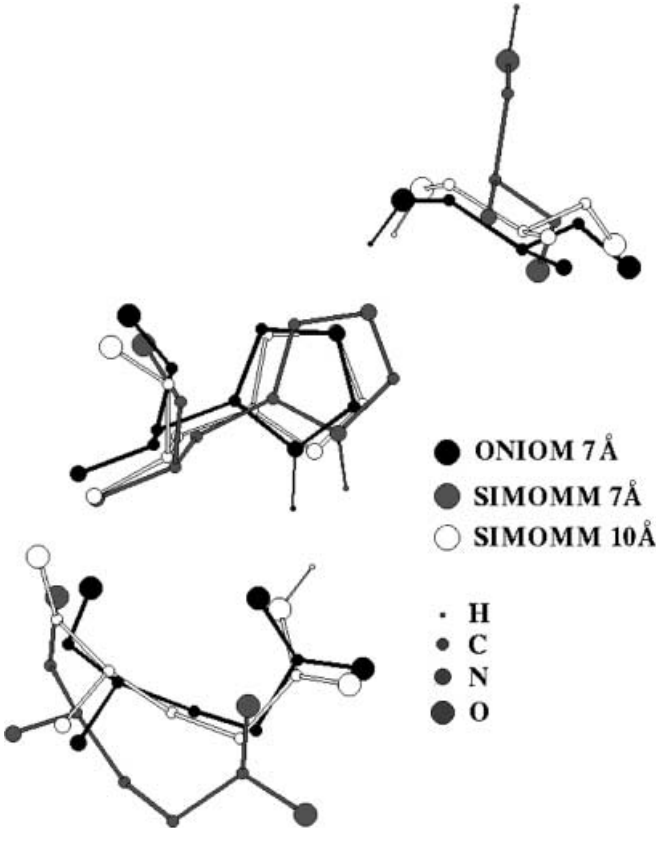

Fig. 3. AChE active-site geometry as a function of different quantum mechanics (*QM*)/molecular mechanics (*MM*) methods (ONIOM versus SIMOMM) and different cluster size (7 versus 10 Å). ONIOM results run at the Hartree–Fock (*HF*)/631G(d) + universal forcefield level; SIMOMM run using HF/631G(d) + AMBER forcefield. All MM atoms are omitted for visual clarity. All hydrogen atoms are also omitted, except the His-H_δ that forms the short, strong hydrogen bond

ONIOM/UFF 7-Å calculation faithfully reproduces the experimentally observed trend (serine alcoholic hydrogen strongly attracted to the histidine ring N; His-H_δ coupled with glutamate) but the SIMOMM/AMBER 7-Å calculation does not display these effects at all. Rather, in the case of the SIMOMM 7-Å calculation, the serine residue angles itself completely away from the histidine such that the alcoholic hydrogen is actually pointing nearly opposite to the expected orientation. The glutamate is also relatively far from the histidine, indicating no effective coupling in this segment either. At the heart of these discrepancies is a tendency for the SIMOMM/AMBER 7-Å representation to cohere relatively poorly in the extended MM bulk region. This effect, not depicted in the much smaller triad pictures herein, involves a partial unraveling of ribbon strands near the periphery of the 7-Å cluster model, apparently allowing the core region to drift slightly apart. Preliminary ONIOM 7-Å calculations (not shown here) using the AMBER forcefield also produced radically different structures from otherwise identical calculations performed with the UFF or DREIDING forcefields.

The shortcomings evident in the 7-Å calculation appear to be largely ameliorated by resorting to a larger model size. In the case of the SIMOMM 10-Å model, a relatively close level of agreement is observed with the qualitatively reasonable ONIOM 7-Å description: strong coupling exists between the serine hydrogen and the histidine ring, and between the His-H_δ and the glutamate. As depicted in Table 1, ONIOM 7-Å results using a range of theory levels and basis set sizes all resulted in a SSHB ranging from 2.49 to 2.62 Å between His-N_δ and the carboxylic oxygen of the glutamate, in excellent agreement with the experimental value of 2.64 ± 0.04 Å. Choice of functional (B3LYP versus. B1LYP) or level of theory (HF versus density functional theory versus second-order Møllet–Plesset) made no significant difference in the structure of the catalytic triad reactants or products. The SIMOMM 10-Å model also demonstrated hydrogen bonding between these residues, although not quite an SSHB. The ONIOM 7-Å model also routinely demonstrates stronger hydrogen bonding between the serine and histidine residues as compared to the SIMOMM 10-Å results. It should be noted that changing the forcefield choice from UFF to DREIDING made no qualitative difference.

In general, the effects of theory level and basis set size are quite minor for both the ONIOM 7-Å and SIMOMM 10-Å cases. The ONIOM 7-Å model consistently shows a minimum-energy triad protonation state of Ser^0–His^-–Glu^0, where the His-H_δ has effectively transferred to the glutamate, while the serine hydrogen does not transfer to the histidine. ONIOM calculations (performed on a smaller model consisting of the active site and oxyanion hole residues only) show a similar general hydrogen-bonding scheme to the larger systems, yet show a minimum-energy protonation state of Ser^0–His^0–Glu^-, similar to previous results [16]. The SIMOMM 10-Å model shows more sensitivity to basis

Table 1. Dependence of structure of catalytic triad in bare enzyme on details of model

Model	High layer	Low layer	SerO–H distance (Å)	SerO–$His N_\epsilon$ distance (Å)	GluO–H distance (Å)	$His N_\delta$–GluO distance (Å)	$His N_\delta$–H-GluO angle (degrees)
ONIOM 7 Å	RHF STO-3G	UFF	1.06	2.61	1.14	2.49	169
ONIOM 7 Å	RHF STO-3G	DREID	1.01	2.65	1.03	2.50	170
ONIOM 7 Å	RHF 6-31G(d)	UFF	0.96	2.84	1.04	2.63	169
ONIOM 7 Å	MP2 STO-3G	UFF	1.09	2.50	1.03	2.63	167
ONIOM 7 Å	RB1LYP STO-3G	UFF	1.06	2.62	1.14	2.49	175
ONIOM 7 Å	RB3LYP STO-3G	UFF	1.06	2.61	1.14	2.49	175
ONIOM bare triad	RB3LYP 6-31G(d,p)	RB3LYP STO-3G	1.05	2.60	1.72	2.73	163
SIMOMM7 Å	RHF 6-31G(d)	AMBER	0.95	5.38	4.34	5.10	135
SIMOMM10 Å	RHF 6-31G(d)	AMBER	0.95	3.11	0.96	2.81	138
SIMOMM10 Å	RHF 6-31G	AMBER	0.96	2.96	0.97	2.67	150
SIMOMM10 Å	RHF 3-21G	AMBER	0.98	2.81	1.86	2.86	175
SIMOMM10 Å	RHF STO-3G	AMBER	0.99	2.84	1.75	2.77	168

set size in that calculations performed with the high layer at RHF STO-3G and RHF 3-21G show a minimum energy state of Ser^0–His^0–Glu^-. Calculations performed with the high layer at RHF 6-31G and 6-31G(d) converge to a protonation state of Ser^0–His^-–Glu^0.

Agent/enzyme calculations

Initial studies to locate TSs included looking at the bare catalytic triad of *T. Californica* AChE with methyl methylphosphonofluoridate, using only QM with Gaussian 98. Two levels of theory, HF/6-31G(d) and B3LYP/6-31G(d), were investigated. The TSs for both levels of theory are depicted in Fig. 4. In the HF/6-31G(d) level of theory, the main contributor to the imaginary frequency is the bond formation between the phosphorous atom and the Ser200 oxygen with minor contribution to the movement of the Ser200 proton moving to the N_{His}.

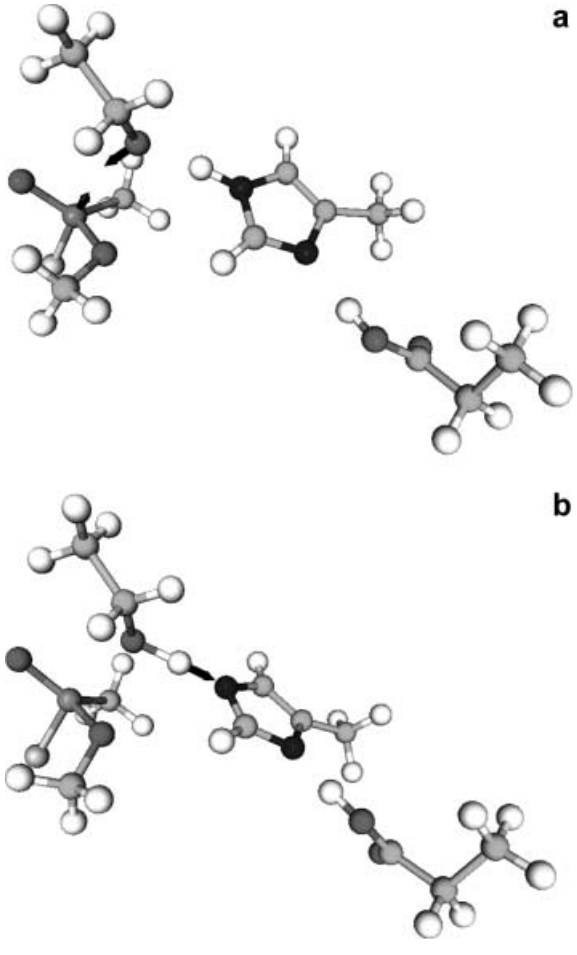

Fig. 4. Comparison of HF (Fig. 4a) and B3LYP (Fig. 4b) QM cluster transition-state results for methyl methylphosphonofluoridate complexing with AChE active site. All relevant atoms are shown; terminal carbon atoms of the serine, histidine and glutamate triad residues have been locked in space; all other atoms were optimized. The dominant contributions to the imaginary frequency are depicted by black arrows

This TS is dubbed a late TS owing to the fact that the proton between the His440 and Glu327 has already formed a bond to the Glu327 with a bond length of 0.98 Å. It is also important to point out that there is no displacement of the proton between His440–Glu327 corresponding to the imaginary frequency in the HF level of theory. The TS barrier for this reaction is quite high at 26.43 kcal/mol. In the B3LYP/6-31G(d) level of theory, the main contributor to the negative frequency is the displacement of the Ser200 proton moving to the His440 nitrogen. At the same time, there are two minor contributions to the imaginary frequency, which include the phosphorus–Ser-O bond formation and the movement of the proton between the Glu-O–His-N_δ. The B3LYP level of theory is considered an earlier TS when compared to the HF level. The distances for the O_{Glu}–N_{His} SSHB in the HF and B3LYP levels are 2.76 and 2.58 Å, respectively. The B3LYP level of theory more accurately shows the simultaneous proton transfers in the catalytic triad and correlates to the empirical SSHB bond distances, as well as demonstrating a significant lowering of the TS barrier to 15.27 kcal/mol.

With the TS found in the cluster calculations, the ONIOM QM/QM methodology was then used to map out energetics of the phosphylation reaction. First, an ONIOM = (HF/6-31G(d):HF/STO-3G) calculation was performed where the terminal methyl group of Glu327 was calculated using the STO-3G basis set and all other atoms were calculated using the 6-31G(d) basis set (not depicted). As earlier, all terminal carbon atoms were frozen in space. The displacement of the TS imaginary frequency was identical to the QM HF level mentioned previously with the major contributor being the phosphorous–O_{Ser} bond formation. This produced a 26.40-kcal/mol reaction barrier that is comparable to the QM HF level discussed earlier and to a rough 30-kcal/mol barrier found in related calculations of phosphonate hydrolysis in aqueous solution (to be reported elsewhere). A second set of calculations was then performed in which the reactant, TS, and product states were located using ONIOM = (B3LYP/6-31G**:B3LYP/3-21G**) where the terminal ethyl group of Glu327 formed the lower layer and all other atoms formed the higher layer (Fig. 5). The displacement of the TS imaginary frequency was identical to the QM density functional theory calculation discussed in the previous paragraph, with the major contributor being the displacement of the Ser200 proton moving to the His440 nitrogen. At the same time, there are two minor contributions to the imaginary frequency, which include the phosphorus–Ser-O bond formation and the movement of the proton between the Glu-O–His-N_δ. There is a 15.18-kcal/mol reaction barrier that is significantly lower than the rough 30-kcal/mol barrier found in related calculations of phosphonate hydrolysis in aqueous solution (to be reported elsewhere). The proper hydrogen-bond scheme is obvious from the structures and an SSHB of 2.59 Å is seen in both the reactant and the product.

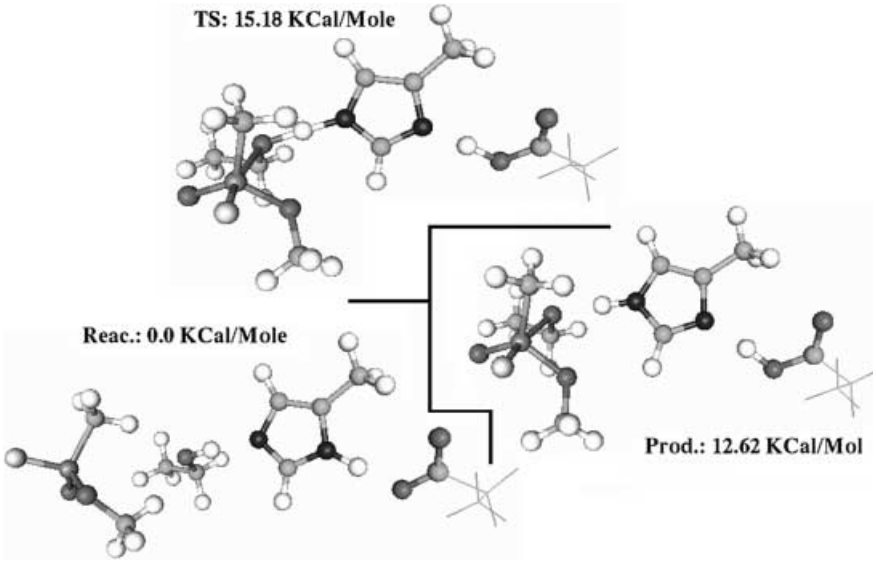

Fig. 5. ONIOM QM/QM [B3LYP/6-31G**:B3LYP/3-21G**] calculations on the initiation state for methyl methylphosphonofluoridate complexation with AChE active-site triad. Structures for the reactants, transition state, and final product are all given, along with corresponding energies relative to the optimized product structure. All relevant atoms are shown, but lower-level (HF/STO-3G) atoms are only given in stick form

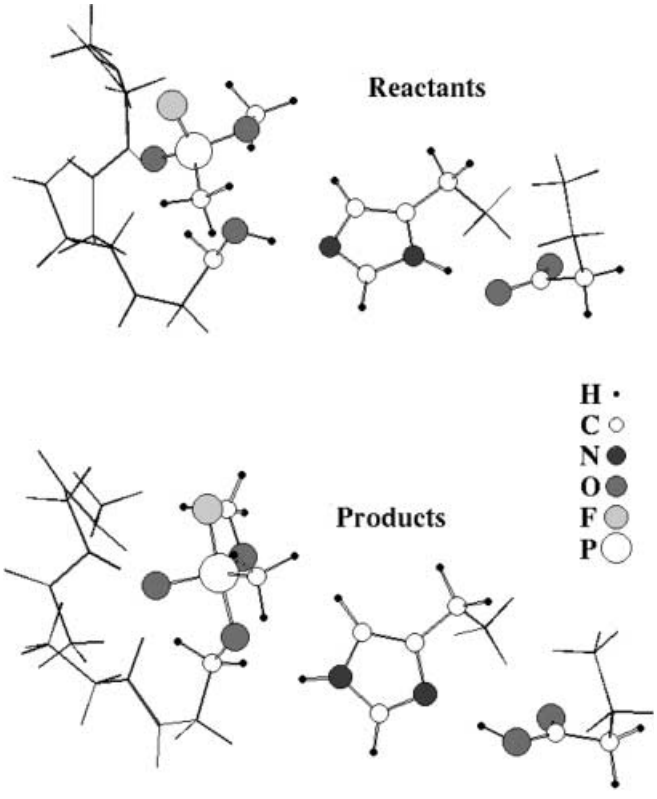

Fig. 6. Reactant and product structures for ONIOM QM/QM [B3LYP/6-31G**; B3LYP/STO-3G] calculations on methyl methylphosphonofluoridate reaction with AChE active site (catalytic triad plus oxyanion hole). All relevant atoms are shown, but lower-level (B3LYP/STO-3G) atoms are only given in stick form. Terminal carbon atoms of all residues were frozen (five carbon atoms total); all others were optimized

Additional residues beside the catalytic triad are postulated to play a role in the phosphylation reaction. The reactant and product of an ONIOM = (B3LYP/6-31G**:B3LYP/STO-3G) QM/QM calculation of the *T. Californica* active-site structure, which includes the oxyanion hole (Gly118, Gly119 and Ala201), is depicted in Fig. 6. It is important to stress that the OP compound is free to move without constraints; however, as depicted in Fig. 6, the phosphonyl bond of the reactant (and product) coordinates in the oxyanion hole (three hydrogens) with the fluorine atom anti to the O_{Ser}. The SSHB distances in the reactant and product are 2.65 and 2.63 Å, respectively. While it is obvious from the reactant structure that the agent orients comfortably into the oxyanion hole before binding to the active site (and properly coordinates with the amide groups of the oxyanion hole backbone), the interaction is still stronger in the product structure. Distances between the substrate oxygen and Gly118, Gly119, and Ala201 amide nitrogens in the product state are around 2.5 Å with a roughly linear hydrogen-bond angle (around 168–175°). Comparison of calculated charges between the product and reactant state show the substrate oxygen to have drawn negative charge in the product state relative to the reactant state, as expected. This important electrostatic stabilization bespeaks the necessity of treating the oxyanion hole residues quantum mechanically. The stereosensitivity of the agent–AChE interactions has been demonstrated experimentally [27], and we have chosen here ostensibly the most reactive forms of the model agents. Investigations of reactions involving different stereoisomers, presentation of different faces of the model agent to the serine residues (and thus affecting orientation into the oxyanion hole and/or steric effects), and steric effects introduced by substitution of branched alkyl and alkoxy groups will be reported elsewhere. Calculations are currently underway to map out energetics of this reaction in the larger 7 and 10-Å models.

A summary of the energetics for the reaction of the model agent with the enzyme at a variety of levels of theory is given in Table 2. The reaction energy is given for completeness, although it must be noted that this will alter significantly with the final removal of the fluoride ion from the complexed system. With removal of the

Table 2. Reactions with model agent methyl-1-methylphosphonofluoridate

System	Treatment	Level of theory/basis set	Transition-state barrier (kcal/mol)	Reaction energy (product–reactants) (kcal/mol)
Bare AChE catalytic triad	QM	RHF/6-31G*	26.43	16.38
Bare AChE catalytic triad	QM	B3LYP/6-31G*	15.27	11.42
Bare AChE catalytic triad	ONIOM	RHF/6-31G*:RHF/STO-3G	26.40	16.35
Bare AChE catalytic triad	ONIOM	B3LYP/6-31G**:B3LYP/3-21G**	15.18	12.62
Oxyanion hole + AChE catalytic triad	ONIOM	B3LYP/6-31G**:B3LYP/3-21G**	No transition state. Work in progress	−1.72

fluoride ion, it has been proposed in previous work [16] that a stable tetrahedral intermediate (TI) is formed, which is highly reminiscent of the reaction of AChE with acetylcholine. In the current work, cluster calculations to date have all shown formation of a trigonal bipyramidal intermediate with fluorine oriented away from the serine, a reasonable preliminary to loss of fluoride and formation of a TI.

Summary and conclusions

This study represents the initial phase of a project devoted to the application of a variety of theoretical methods to investigate reactions of model nerve agents in the active site of AChE. Mixed QM/MM methods have been used to estimate the sensitivity of the catalytic triad of the bare enzyme to details of the model. Effects of forcefield choice cannot be decoupled from effects of methodology (SIMOMM versus ONIOM) at this point, so the overall effect of user-defined constraints on results is yet to be determined for this system. In this series of results, the AMBER forcefield has largely proven problematic. However, both methodologies do yield results with excellent alignment of the catalytic triad, and the ONIOM models have successfully reproduced the SSHB seen experimentally. Dependence on basis set size and level of theory has largely been manifested in subtle details of the hydrogen-bonding pattern.

We have begun achieving insight into the reactions of model nerve agent species with the AChE active site. In small QM cluster studies, we have successfully isolated a TS and optimized structure for the nucleophilic complexation of a nerve agent analog by the serine residue in the active site. These results successfully demonstrate both of the expected serine → histidine and histidine → glutamate proton transfers in conjunction with the serine binding the agent. This is also seen in larger QM and QM/QM calculations, which predict a significantly reduced activation barrier for the complexation reaction: 15.18 kcal/mol rather than approximately 30 kcal/mol as was predicted from QM calculation of the explicit 2-water hydrolysis of methyl methylphosphonofluoridate at the B3LYP/6-311 + G(2d,2p) level (publication in preparation). In addition, the direct involvement of the oxyanion hole residues (here treated quantum mechanically) is shown. This significant barrier reduction and additional residue involvement is obvious evidence of the highly reactive nature of the enzyme-activated process and is evidence for the capacity of our calculations to reproduce some experimentally expected behavior.

We have demonstrated the utility of these methods in reproducing physical details of the system that affect the relative toxicity of existing agents. More importantly, we will subsequently be able to use this knowledge to predict chemical therapeutic and prophylaxic mechanisms for threat mitigation and will be able to anticipate prospective new nerve agent formulations of possible future threat to our military objectives and civilian well-being.

References

1. Taylor P, Brown JH (1994) Basic neurochemistry: molecular, cellular, and medical aspects, 5th edn. Raven, New York, pp 231–260
2. Eto M (1974) Organophosphorus pesticides: organic and biological chemistry. CRC, Boca Raton
3. Heilbronn E (1993) In: Cholinergic Function and Dysfunction. Elsevier, NY pp 133–138
4. Schwartz JH (1985) Principles of neural science, 2nd edn. Elsevier, New York, pp 159–168
5. Harel M, Quinn DM, Nair HK, Silman I, Sussman JL (1996) J Am Chem Soc 118:2340–2346
6. Broomfield CA, Lockridge O, Millard CB (1999) Chem Biol Interact 119–120:413–418
7. Millard CB, Kryger G, Ordentlich A, Greenblatt HM, Harel M, Raves ML, Segall Y, Barak D, Shafferman A, Silman, Sussman JL (1999) Biochemistry 38:7032–7039
8. Somani SM, Romano JAJ (2001) In: Chemical warfare agents: toxicity at low levels. CRC, Boca Raton, and references therein
9. Doctor BP, Taylor P, Quinn DM, Rotundo RL, Gentry MK (1999) In: Structure and function of cholinesterases and related proteins. Kluwer/Plenum, Dortrecht, and references therein
10. Daggett V, Schroder S, Kollman P (1991) J Am Chem Soc 113:8926–8935
11. Albaret C, Lacoutiere S, Ashman WP, Froment D, Fortier P-L (1997) Protein Struct Funct Genet 28:543–555
12. Fuxreiter M, Warshel A (1998) J Am Chem Soc 120:183–194
13. Bencsura A, Enyedy IY, Kovach IM (1996) J Am Chem Soc 118:8531–8541
14. Tai K, Shen T, Borjesson U, Philippopoulos M, McCammon JA (2001) Biophys J 81:715–724
15. Shen TY, Tai K, McCammon JA (2001) Phys Rev E 63:041902, and references therein
16. Vasilyev VV (1994) J Mol Struct (THEOCHEM) 304:129–141
17. Mulholland AJ, Lyne PD, Karplus M (2000) J Am Chem Soc 122:534–535
18. Topf M, Varnai P, Richards WG (2001) Theor Chem Acc 106:146–151

19. Dapprich S, Komaromi I, Byun KS, Morokuma K, Frisch MJ (1999) J Mol Struct (THEOCHEM) 461:1–21, and references therein
20. Shoemaker J, Burggraf LW, Gordon MS (1999) J Phys Chem A 103:3245–3251
21. Maseras F, Morokuma K (1995) J Comput Chem 16:1170–1180
22. Gaussian 98, revision A.7. Frisch MJ, Trucks GW, Schlegel HB, Scuseria GE, Robb MA, Cheeseman JR, Zakrzewski VG, Montgomery JA, Stratmann RE, Burant JC, Dapprich S, Millam JM, Daniels AD, Kudin KN, Strain MC, Farkas O, Tomasi J, Barone V, Cossi M, Cammi R, Mennucci B, Pomelli C, Adamo C, Clifford S, Ochterski J, Petersson GA, Ayala PY, Cui Q, Morokuma K, Malick DK, Rabuck AD, Raghavachari K, Foresman JB, Cioslowski J, Ortiz JV, Stefanov BB, Liu G, Liashenko A, Piskorz P, Komaromi I, Gomperts R, Martin RL, Fox DJ, Keith T, Al-Laham MA, Peng CY, Nanayakkara A, Gonzalez C, Challacombe M, Gill PMW, Johnson BG, Chen W, Wong MW, Andres JL, Gonzalez C, Head-Gordon M, Replogle ES, Pople JA (1998) Gaussian Inc., Pittsburgh, PA
23. Schmidt MW, Baldridge KK, Boatz JA, Jensen JA, Koseki JH, Matsunaga N, Gordon MS (1993) J Comput Chem 14:1347–1363
24. Pappu RV, Hart RK, Ponder JW (1998) J Phys Chem B 102:9725–9744, and references therein
25. Viragh C, Harris TK, Reddy PT, Massiah MA, Mildvan AS, Kovach IM (2000) Biochemistry 39:16200–16205
26. Bourne Y, Taylor P, Bougis PE, Marchot P (1999) J Biol Chem 274:2963–2970
27. Ordentlich A, Barak D, Kronman C, Benschop HP, De Jong LPA, Ariel N, Barak R, Segall Y, Velan B, Shafferman A (1999) Biochemistry 38:3055–3066